EurJIC
European Journal of Inorganic Chemistry

Full Papers
doi.org/10.1002/ejic.202100453

Chemistry Europe
European Chemical Societies Publishing

www.eurjic.org

Hydrolysis of Uranyl-, Nd-, Ce-Ions and their Mixtures by Thermal Decomposition of Urea

Christian Schreinemachers,*[a, b, c] Olivier Bollen,[c] Gregory Leinders,[b] Václav Tyrpekl,[d] Giuseppe Modolo,[a] Marc Verwerft,[b] Koen Binnemans,[c] and Thomas Cardinaels[b, c]

The hydrolysis of uranyl-, Nd- and Ce-cations, induced by thermal decomposition of urea was investigated and the impact of the urea content and the experiment temperature on the reaction kinetics was evaluated. Uranyl precipitated as ammonium diuranate (ADU) with varying stoichiometry. Nd(III) and Ce(III) showed comparable pH evolutions and lanthanide carbonate hydroxide ($LnCO_3OH$) products were identified, whereas Ce(IV) hydrolysed at lower pH and formed CeO_2. The precipitation behaviour was confirmed for mixtures of uranyl and the lanthanides. Depending on the urea content, a partial co-precipitation occurred in U/Nd mixtures. The phases formed with Ce(III) and Ce(IV) were also identified in the precipitates of binary U/Ce mixtures. In ternary U/Nd/Ce compositions, a simultaneous precipitation of Nd(III) and Ce(III) was observed and a partial incorporation of the lanthanides into the ADU phase, whereas the precipitation in the presence of Ce(IV)/CeO_2 led to the formation of three individual phases.

1. Introduction

Partitioning and transmutation is a key strategy to reduce spent nuclear fuels' radiotoxicity and heat generation.[1] Long-lived minor actinides (MAs) are partitioned from spent nuclear fuel and subsequently converted into precursors to manufacture fuel pins or target materials. These types of nuclear fuel can be used in fast reactor systems to fission the MAs into short-lived radioisotopes. An essential link between the partitioning and the transmutation is the conversion of the separated MAs into solid precursors to fabricate fresh fuel suitable for MA recycling. Besides conventional powder processing, the reference process for ceramic nuclear fuel production (UO_2 and $(U,Pu)O_2$), sol-gel processes were explored to avoid handling of fine powder and to facilitate automation for the production of nuclear fuel particles.[2] In the sol-gel process a spherically shaped precipitate is formed and thermally converted into an oxide, which can directly be used as particle fuel[3] or compressed into the commonly used fuel pellets.[4]

The feasibility of the sol-gel route via internal gelation (IG) was demonstrated for the preparation of Nd- and Ce-doped UO_2 microspheres,[5,6] with Nd and Ce acting as Am and Pu surrogates, respectively. Cerium was used in its trivalent and tetravalent state as dopant precursor and depending on the oxidation state of the dopant precursor a significantly different behaviour during the conversion into $U_{1-y}Ln_yO_{2\pm x}$ was observed.[7]

Akinc and Sordelet[8] investigated the hydrolysis reactions of Nd(III) and Ce(III) ions from nitrate solution by thermal decomposition of urea at ambient pressure. The precipitation is triggered by ammonia formation due to the decomposition of urea, bicarbonate is generated additionally, as shown in equation (1).[9]

$$CO(NH_2)_2 + H^+ + 2H_2O \rightarrow HCO_3^- + 2NH_4^+ \quad (1)$$

Wang and Lu[10] adopted the method, used hydrothermal conditions, and a feed stock solution of $Ce(NO_3)_3$. This approach was also applied to study the hydrolysis behaviour of $UO_2(NO_3)_2$ (90 °C and 120 °C).[11] The results of both studies demonstrate an influence of the urea content, temperature, and treatment time on the morphology of the formed precipitates.

Within this work, the hydrolysis of uranyl ions (UO_2^{2+}) and lanthanide ions (Nd(III), Ce(III), Ce(IV)), induced by thermal decomposition of urea, was investigated. The precipitation behaviour of the individual ions, as well as their mixtures, was studied to gain more insight in the hydrolysis, which causes the solidification in the IG process.

2. Results

Hydrolysis experiments were performed using aqueous solutions containing the individual metal ions (UO_2^{2+}, Nd(III), Ce(III)

[a] Dr. C. Schreinemachers, Prof. Dr. G. Modolo
Forschungszentrum Jülich GmbH, Institute of Energy and Climate Research (IEK), IEK-6: Nuclear Waste Management and Reactor Safety
52425 Jülich, Germany
E-mail: c.schreinemachers@fz-juelich.de
[b] Dr. C. Schreinemachers, Dr. G. Leinders, Dr. M. Verwerft, Prof. Dr. T. Cardinaels
Belgian Nuclear Research Centre (SCK CEN), Institute for Nuclear Materials Science
Boeretang 200, B-2400 Mol, Belgium
[c] Dr. C. Schreinemachers, O. Bollen, Prof. Dr. K. Binnemans, Prof. Dr. T. Cardinaels
KU Leuven, Department of Chemistry
Celestijnenlaan 200F, P.O. Box 2404, B-3001 Heverlee, Belgium
[d] Dr. V. Tyrpekl
Charles University in Prague, Department of Inorganic Chemistry
Hlavova 2030/8, 128 43 Prague 2, Czech Republic

or Ce(IV)). Binary compositions of UO_2^{2+}/Nd(III), UO_2^{2+}/Ce(III), and UO_2^{2+}/Ce(IV) were studied, as well as the ternary system with the three elements, using the Ce(III) and Ce(IV) precursor, respectively. The conditions applied during the hydrolysis experiments were adopted from Wangle et al.,[12] who investigated the homogeneous hydrolysis of thorium by thermal decomposition of urea at 90 °C and 100 °C using molar amounts of urea corresponding to 5, 25 and 50 times the molar Th content (c(Th) = 0.05 mol L^{-1}). The hydrolysis reactions were followed-up by pH measurements, ultraviolet-visible spectroscopy (UV/Vis), and inductive coupled plasma mass spectrometry (ICP-MS) and the precipitates were characterised by X-ray powder diffraction (XRD) and scanning electron microscopy (SEM).

2.1. Reaction follow-up

2.1.1. pH measurements

The pH values measured during the hydrolysis experiments with uranyl and without any metal are summarised in Figure 1. For the experiments without metal ions, we observed a starting pH of 6.60, followed by a steep increase up to pH 8.05 within 70 min. Afterwards, the pH increased linearly by about 0.134 per 100 min up to 412 min. Within the next 60 min, the pH of the solution increased to the final pH of 8.81.

Experiments with uranyl ions and $R = 26$ $\left(= \frac{n(\text{urea})}{n(M^{n+})}\right)$ were carried out at temperatures of 90 °C and 100 °C. At 90 °C, an additional experiment was performed with $R = 52$ (Figure 1). The initial pH, prior to the urea addition ranged between 2.53 and 2.84. Upon urea addition, an increase to pH values between 3.83 and 4.07 was observed and the solutions' yellow colour became significantly more intense. At a pH of about 5 the creation of precipitate was visually observed for all three conditions, this is consistent with the formation of a plateau in the plots. For $R = 26$, the pH increase took 77 min and 225 min at 100 °C and 90 °C, respectively. Whereas for R of 52 at 90 °C it was reached 101 min after the urea addition. During the precipitation, the intensity of the solutions' colour decreased and they were colourless after exceeding a pH of about 6.3. This agrees to the trends shown in Figure 1, where the plateau is ending and a more rapid pH increase is notable for values above 6. It occurred before the sampling at 127 min (100 °C) and 373 min (90 °C) after urea addition ($R = 26$). For the experiment with $R = 52$ it was noticed at a higher pH (7.49) before the sampling at 251 min. At the last sampling of the same day, comparable pH values of 7.90, 7.96 and 7.98 were measured, which slightly increase during the night to final values of 8.03, 8.37 and 8.16.

Since a temperature of 90 °C and a urea content of 26 times the molar metal amount were suitable to follow the reaction in an appropriate time frame, those conditions were chosen to investigate the precipitation behaviour of Nd(III), Ce(III) and Ce(IV) ions. The obtained pH curves and the already described data for uranyl, using the mentioned conditions, are compared in Figure 2a.

The trivalent Nd and Ce ions showed a comparable behaviour, initial pH values of 5.06 and 4.98 were measured, which increased after urea addition to 5.92 and 5.60, respectively. The formation of a white precipitate was observed during the first sampling at about 25 min for both elements. For the experiment with Nd(III), the pH fluctuated between 5.7 and 6.0 during the precipitation. At 449 min the pH reached 6.28 and increased to 7.66 after 550 min. For the experiment with Ce(III), an increase in pH was observed during the precipitation, reaching 6.27 at 547 min. Final pH values of 8.27 and 8.22 were measured, respectively.

A significantly different behaviour was observed for Ce(IV) ions. The initial pH was 1.26, which increased due to the addition of urea to 1.65 (25 min), after 50 min a pH value comparable to the initial one was measured (1.31). Unlike the trivalent lanthanides, no precipitation was visually observed at this point. The pH gradually evolved to 2.93 after 7.5 hours and then steeply rose to 6.06 over the next fifty minutes. The latter

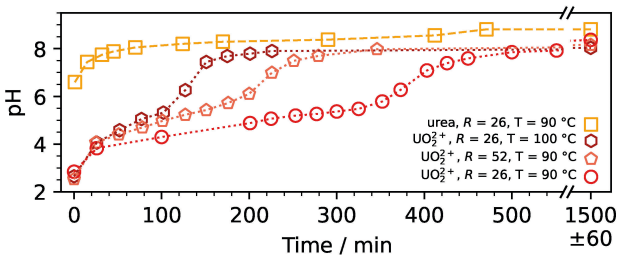

Figure 1. Measured pH as a function of time during the hydrolysis experiments with 0.05 mol L^{-1} $UO_2(NO_3)_2$ at different temperatures and urea contents, as well as the pH development for a solution containing only urea at 90 °C (concentration equal to $R = 26$ experiments).

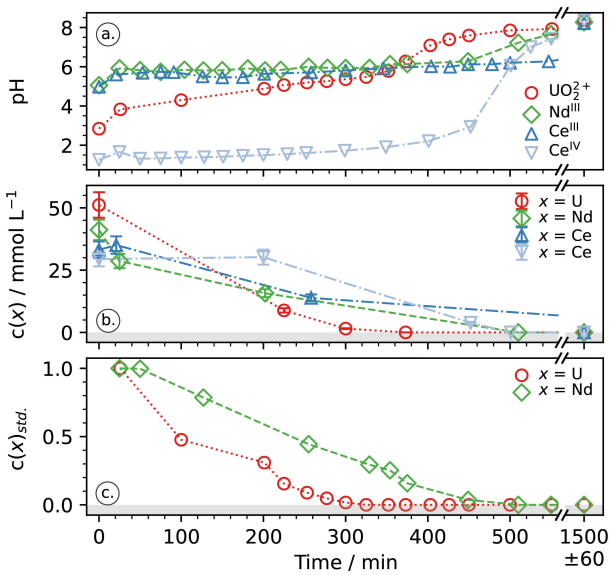

Figure 2. (a) pH evolution during hydrolysis reaction of single components at 90 °C and $R = 26$. (b) Evolution of the molar metal concentrations determined by ICP-MS, and (c) metal evolutions normalised to their initial concentration (UV/Vis results).

rapid pH increase went along with the formation of white precipitate. Afterwards, the pH continued to increase, reaching 7.42 at 550 min and 8.37 in the final sample.

The described trends of the individual ions were also observed for binary mixtures of uranyl with the lanthanides. Four different conditions were applied to mixtures of UO_2^{2+} and Nd(III). Nd molar metal fractions of 10 mol% and 25 mol% were used, each with R of 26 and 52 at 90 °C. Figure 3a and 3d show the development of the pH during the experiment with 10 mol% Nd and both urea contents, respectively. For $R=26$, the initial pH of 2.94 increased to 3.77 (24 min) upon urea addition and then linearly to 5.04 (199 min, Figure 3a). It is followed by a slight increase up to 5.55 (303 min), before rapidly rising to 7.02 (406 min). For $R=52$, a comparable trend was observed, but in this case the plateau was shorter and the entire reaction occurred much faster, as it was also observed for the single component system with uranyl ions (Figure 1). Figure 3d shows a rapid pH increase to 4.14 (26 min) upon urea addition, followed by a plateau reaching 4.95 at 126 min. Afterwards a fast increase to 7.00 at 228 min took place. The pH during the experiments with 25 mol% Nd behaved similarly, but in this case the initial increase was slower and the increase from pH values of about 5 to about 7 took longer. A Figure comparable to Figure 3 showing the results for 25 mol% Nd is part of the dataset of this study (Figure 5 within Ref. 13).[13]

The hydrolysis of mixtures of UO_2^{2+} and Ce in both oxidation states with $R=26$ at 90 °C was also investigated, plots of the pH as function of time can be found in the dataset as well (Figure 6 within Ref. 13).[13] For both oxidation states, mixtures of uranyl and Ce ions with Ce contents of 20 mol% were investigated, confirming also the findings of the individual metal ions. The usage of trivalent Ce resulted in a comparable curve to the one with Nd, showing an increase from pH 3.00 to 3.86 (25 min) after the addition of urea. It increased linearly to pH 5.20 (199 min), followed by a quite stable pH up to 299 min, which increased then to pH 6.80 (407 min). For the mixture of UO_2^{2+} and Ce(IV), the initial pH of 1.49 reached 2.05 (25 min) upon urea addition and increased further to 2.50 (75 min), followed by a steep increase to pH 4.02 (150 min) and a slow increase to pH 5.12 (301 min). A pH ranging between 8.2 and 8.3 was measured in the final samples of the binary UO_2^{2+} and Ce compositions.

A combination of the described behaviour was observed for the ternary systems consisting of 55 mol% UO_2^{2+}, 25 mol% Nd(III) and 20 mol% Ce(III) or Ce(IV), respectively. It is presented in Figure 4a and 4c. For the experiment with uranyl and both trivalent lanthanides, a pH of 5.89 is reached at 200 min, followed by a quite long plateau ranging between pH 6.35 (230 min) and 6.48 (377 min). Whereas for the experiment with tetravalent Ce a plateau ranging between pH 2.41 (25 min) and 2.67 (75 min) is followed by a slowly increasing pH region from 4.04 (125 min) to 5.30 (227 min) and a short plateau of pH 6.36 (300 min) to pH 6.68 (381 min).

2.1.2. ICP-MS measurements

The uranium concentration of certain samples was determined via ICP-MS. Uranium concentrations decreased with increasing time. At 127 min, 251 min and 373 min no uranium was measured in the supernatant for the experiments carried out with $R=26$ (100 °C), $R=52$ (90 °C), and $R=26$ (90 °C), respectively. The data for the latter are shown in Figure 2b, together with the results measured for the individual lanthanides, confirming the precipitation plateaus described previously.

The ICP-MS results for the UO_2^{2+} and Nd(III) mixtures with 10 mol% Nd are included in Figure 3. For both urea contents we observe first a decrease in the U concentration, followed by a decrease in the Nd concentration. No uranium was measured

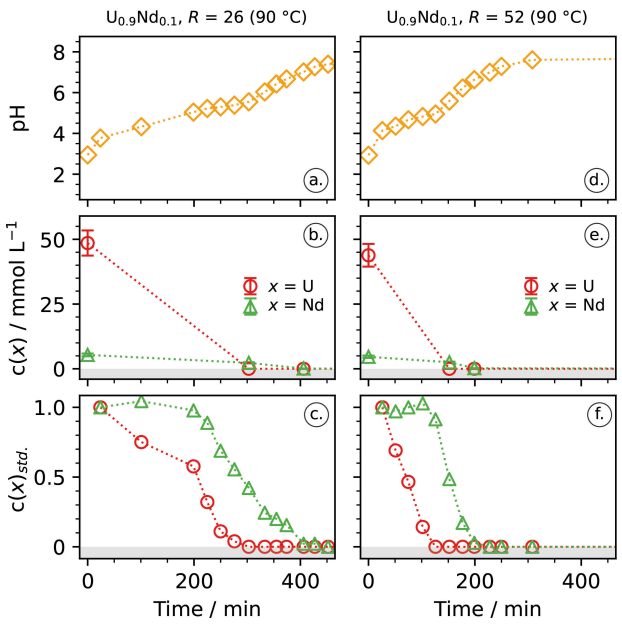

Figure 3. Development of the pH during the hydrolysis of UO_2^{2+} and Nd(III) for binary compositions with 10 mol% Nd (a, d), performed at 90 °C with R of 26 and 52, molar metal concentrations determined by ICP-MS (b, e), as well as standardised concentrations determined by UV/Vis (c, d).

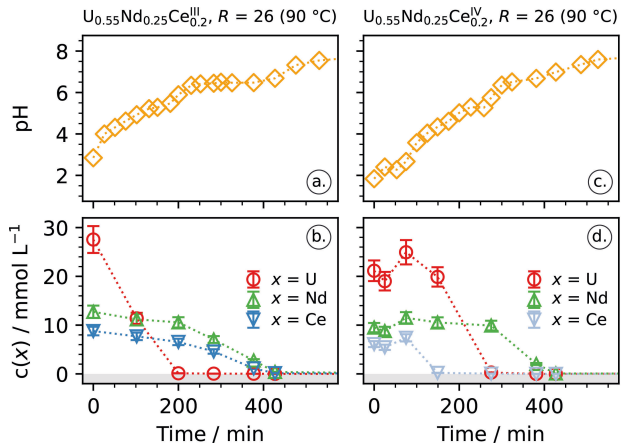

Figure 4. Development of the pH during the hydrolysis reactions for ternary compositions with Ce(III) and Ce(IV) precursor (a, c) performed at 90 °C with $R=26$ and the molar metal concentrations determined by ICP-MS (b, d).

in samples taken at 303 min ($R=26$, Figure 3b) and 152 min ($R=52$, Figure 3e), while 43 % and 54 % of the initially measured Nd was still present in the supernatant of those samples. In the samples taken at 406 min ($R=26$) and 199 min ($R=52$), no Nd was measured. Results of compositions with a Nd content of 25 mol% in the mixtures confirmed the trends for both urea contents. At 253 min ($R=26$) and 99 min ($R=52$) the supernatant was free of U, while Nd was still present (72.1 % and 73.0 %). For $R=26$, only the final sample was additionally analysed by ICP-MS, showing no remaining Nd, whereas for $R=52$ already after 228 min no Nd was detected by ICP-MS in the supernatant indicating a complete precipitation.

Mixtures of the binary system UO_2^{2+} and Ce using Ce(III) and Ce(IV) were also characterised by ICP-MS. The experiment with trivalent Ce (20 mol%) behaved comparable to the UO_2^{2+}/Nd(III) mixtures, in the sample where no U was measured, Ce was still measured (331 min, 29.9 %), which was not present in the final sample any more. In the first two samples of the experiment with tetravalent Ce (20 mol%) both elements were still present with concentrations comparable to the initial one, while none of the elements were measured in the third analysed sample (325 min). However, ICP-MS results of the ternary system $U_{0.55}Nd_{0.25}Ce_{0.2}$ revealed that Ce(IV) precipitated prior to UO_2^{2+}. The results are shown in Figure 4b and 4d for the Ce(III) and Ce(IV) precursors, respectively. The experiment performed with the trivalent lanthanide precursors shows a precipitation of the uranyl ions, followed by a simultaneous precipitation of Nd(III) and Ce(III). The molar metal concentration for both lanthanides decreased proportionally (Figure 4b). For the experiment with tetravalent cerium, we observed three individual precipitation reactions, starting with Ce(IV), followed by UO_2^{2+} and finally for Nd(III) (Figure 4d).

2.1.3. UV/Vis measurements

The UV/Vis spectrum of the uranyl nitrate solution is presented for the wavelength range between 375 nm and 505 nm in Figure 5a. An absorption maximum was measured at 414 nm (dashdotted line). Moreover, the spectrum measured in the first sample after urea addition (26 min, $R=26$, $T=90$ °C) is shown in Figure 5a. The urea addition caused a shift of the absorption maximum to a wavelength of 421.5 nm, paired with an increase in intensity. During the experiment, the intensity decreased as presented for certain samples in Figure 5b. The solution sampled 325 min after urea addition ($R=26$, 90 °C) showed no absorbance in the wavelength region of interest. For the experiment performed with $R=52$ (90 °C), this occurred in the sample taken at 127 min. Due to instabilities, it was not possible to perform this analysis with the samples of the experiment performed at 100 °C. The absorbance measured at 421 nm was normalised to the absorbance observed for the first sample containing urea (26 min), the results for $R=26$ (90 °C) are shown as function of time in Figure 2c.

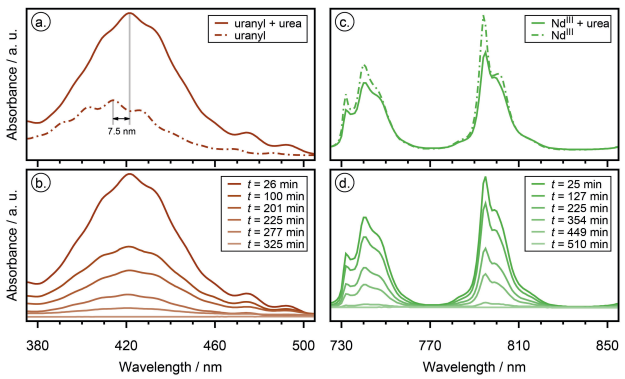

Figure 5. UV/Vis spectra of the solution prior to the hydrolysis with and without urea, as well as the spectra of selected samples during the hydrolysis for experiments with uranyl (a,b) and Nd(III) (c,d) at 90 °C with $R=26$.

The UV/Vis spectrum of the $Nd(NO_3)_3$ solution for the range between 725 nm and 855 nm is shown in Figure 5c. Urea addition led to a decrease in absorbance, most likely caused by the volume increase due to its dissolution. No wavelength shift occurred and peak maxima were observed at 740 nm and 794 nm, additional ones occurred at 522 nm, 575 nm and 865 nm, which are not included in Figure 5c + d. The intensity decreased during the experiment (Figure 5d) and no absorption was measured at 510 min and later on. Figure 2c includes the Nd absorbance measured at 794 nm normalised to the absorbance of the first sample containing urea (25 min).

The UV/Vis data obtained for UO_2^{2+} and Nd(III) mixtures were processed in the same way and the results of the compositions with 10 mol% Nd are presented as Figure 3c and Figure 3f for $R=26$ and 52, respectively. For both urea contents we observe a decrease in UO_2^{2+} concentration followed by a decreasing Nd(III) concentration. During the experiment with $R=26$ there is an overlapping region where both ions precipitate (200 min to 300 min), while for $R=52$ the precipitation of UO_2^{2+} was completed before Nd(III) started precipitating. Moreover, we recognised that the doubling of the urea content speeded the precipitation up by a factor of two. Similar observations were made for binary mixtures with 25 mol% Nd, a Figure showing those results is part of the dataset of this study (Figure 5 within Ref. 13).[13]

A UV/Vis spectrum of Ce(III) shows a maximum absorbance at 265 nm with a shoulder up to about 350 nm,[14] overlapping with the NO_3^- absorbance having a maximum at 220 nm and a broad absorption band up to about 340 nm.[15] The spectra were reproduced in our samples, but a deconvolution of the data for the Ce cations and NO^- anions was kept out of scope of this study. However, the ICP-MS results for the ternary system (Figure 4b) demonstrated a comparable precipitation behaviour of Ce(III) and Nd(III). Also for the experiments containing Ce(IV), the processing of the UV/Vis data was more difficult due to a very broad absorption up to about 500 nm,[16,17] influencing also the UO_2^{2+} absorption. Similar as for the Ce(III) experiments, we could rely on the ICP-MS measurements (Figure 4d), which clearly demonstrated the precipitation of Ce(IV) prior to UO_2^{2+}, therefore no further deconvolution of those data was performed. However, the UV/Vis results obtained for the experiments containing both Ce precursors are included in the dataset.[13]

2.2. Characterisation of precipitates

2.2.1. XRD analyses

The XRD patterns obtained for the precipitates of the single component experiments are summarised in Figure 6, showing the results for the UO_2^{2+} precipitates in subfigures 6a–c. $2UO_3 \cdot NH_3 \cdot 3H_2O$ (PDF-2: 00-044-0069),[18] $3UO_3 \cdot NH_3 \cdot 5H_2O$ (PDF-2: 00-043-0365)[18] and/or $UO_3 \cdot 2H_2O$ (PDF-2: 00-043-0364)[18] were assigned to the obtained patterns. The precipitate formed with $R = 26$ at 100 °C is biphasic, the majority phase was $2UO_3 \cdot NH_3 \cdot 3H_2O$ and a smaller fraction of $3UO_3 \cdot NH_3 \cdot 5H_2O$ was found (Figure 6a). A temperature reduction to 90 °C and urea increase to $R = 52$ resulted in a biphasic product as well, having $2UO_3 \cdot NH_3 \cdot 3H_2O$ as majority phase and $UO_3 \cdot 2H_2O$ as by-product (Figure 6b), whereas half of the urea content at the same temperature ($R = 26$) led to a monophasic $2UO_3 \cdot NH_3 \cdot 3H_2O$ precipitate (Figure 6c) with a hexagonal crystal system. Lattice parameters of $a = b = 1.410(4)$ nm and $c = 1.451(4)$ nm were determined, which are consistent with the lattice parameters published by Debets and Loopstra (PDF-2: 00-044-0069).[18]

The results for the individual lanthanide precipitates formed with $R = 26$ at 90 °C are presented as Figure 6d–f. For the experiments with the trivalent lanthanides, neodymium hydroxy carbonate ($NdCO_3OH$, PDF-2: 00-027-1296,[19] Figure 6d) and cerium hydroxy carbonate ($CeCO_3OH$, PDF-2: 00-041-0013,[8] Figure 6e) with an orthorhombic crystal system were identified as products. The lattice parameters were determined as $a = 0.503(4)$ nm, $b = 0.849(8)$ nm, $c = 0.733(6)$ nm for the $NdCO_3OH$ and $a = 0.500(2)$ nm, $b = 0.856(4)$ nm, $c = 0.731(2)$ nm for the $CeCO_3OH$. In both cases, these correspond to the reference lattice parameters published in PDF-2: 00-027-1296,[19] and PDF-2: 00-041-0013.[8]

The usage of Ce(IV) resulted in a cerium dioxide precipitate (CeO_2, PDF-2: 00-034-0394,[20] Figure 6f). The diffractogram shows broad reflections and a poor peak-to-background level. CeO_2 nanocrystals with a mean crystallite size of 7 nm and a microstrain of 0.05 % were determined via the Williamson-Hall method.[21]

The XRD patterns measured for the binary component precipitates are summarised in Figure 7. The results obtained for mixtures of UO_2^{2+} and Nd(III) with $R = 52$ are shown in subfigures 7a + b. We observed a precipitate with poor crystallinity and an amorphous fraction for the mixture with a Nd content of 10 mol% (Figure 7a). However, it indicates reflections at the 2θ angles where they were also recognised for the ammonium diuranate (ADU) compound obtained with $R = 52$. For the Nd content of 25 mol% (Figure 7b) a significantly better crystallinity was determined. The reflections are not as sharp as the ones measured for the individual phases of the single component experiment, but they occur at comparable 2θ positions. The pattern is dominated by the ADU reflections, but the four major reflections of the $NdCO_3OH$ phase are clearly

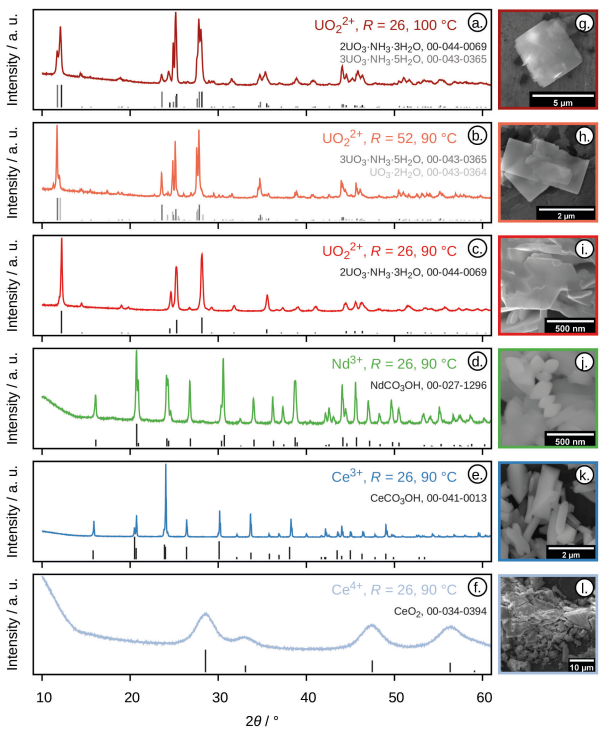

Figure 6. X-ray diffraction pattern and SEM micrographs obtained for the precipitates formed during the hydrolysis experiments with the single components UO_2^{2+}, Nd(III), Ce(III) and Ce(IV), as well as reference patterns originating from the PDF-2 database.[8,18–20]

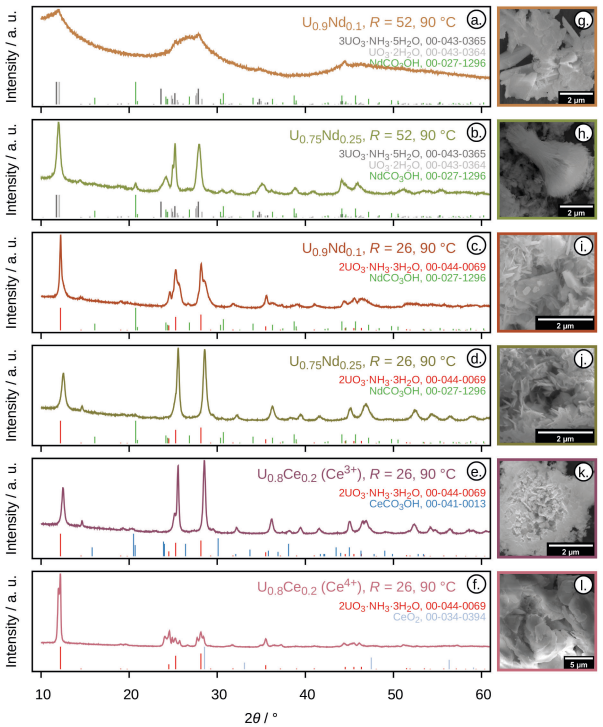

Figure 7. X-ray diffraction pattern and SEM micrographs obtained for the precipitates formed during the hydrolysis experiments for the binary systems containing mixtures of UO_2^{2+}/Nd(III) (10 mol% and 25 mol% Nd), UO_2^{2+}/Ce(III) and UO_2^{2+}/Ce(IV) (20 mol% Ce), and reference patterns from the PDF-2 database.[8,18–20]

recognisable (20.7°, 24.2°, 26.7° and 30.6°), indicating the presence of two individual phases.

The results of the precipitates for both compositions prepared with $R=26$ are shown in Figure 7c+d. In this case a much better crystallinity was obtained for the mixture with 10 mol% Nd, as compared to the precipitate prepared with $R=52$. The reflections of the $2UO_3 \cdot NH_3 \cdot 3H_2O$ phase were observed as well, they exhibit a shoulder indicating the presence of ADU phases with different stoichiometry (compare Figure 6a+b). Reflections of the Nd phase could not be assigned to the pattern, but assuming the stoichiometry observed for the individual components it has a mass fraction of 7.1 wt% only. The mixture with a Nd content of 25 mol% (Figure 7d) resembles the pattern of the $2UO_3 \cdot NH_3 \cdot 3H_2O$ phase (Figure 6b). The $NdCO_3OH$ phase (18.7 wt%) is not as emphasised as in the precipitate formed with $R=52$ (Figure 7b), but at a closer look the reflection with the highest intensity at 20.7° it is observed.

The XRD results of the precipitates containing 20 mol% Ce are shown as Figure 7e and 7f ($R=26$), for the Ce(III) and Ce(IV) precursor, respectively. The pattern obtained for the mixture prepared with the trivalent Ce looks comparable to the one measured for UO_2^{2+}/Nd(III) (25 mol% Nd, Figure 7d). The reflections indicate a better crystallinity, even though a lower mass fraction of 14.4 wt% for the $CeCO_3OH$ phase is present in the mixture, the reflection at about 20.3° is recognisable in the pattern. For all mixtures prepared with the trivalent *Ln* precursors, a shift of the ADU reflections towards higher 2θ angles was observed, indicating a partial implementation of the *Ln* element into the ADU matrix in addition to the individual hydroxycarbonate phases. This shift was not found for the mixture prepared with UO_2^{2+}/Ce(IV) and additional reflections to those of the $2UO_3 \cdot NH_3 \cdot 3H_2O$ phase were observed, indicating the presence of ADU phases with different stoichiometry (compare Figure 6a+b). The CeO_2 phase is not visible in the mixture despite having a mass fraction of 11.8 wt%, which can be explained by its nanocrystallinity (compare Figure 6f).

The XRD results obtained for the ternary mixtures are presented along with the reference patterns in Figure 8. Reflections of the individual *Ln* phases are visible, they are more emphasised than in the results obtained for the binary mixtures, which might be due to the smaller mass fractions of the ADU phase (64.2 wt% and 66.3 wt%). However, the patterns of the $2UO_3 \cdot NH_3 \cdot 3H_2O$ phase exhibit for the precipitate from both experiments a shift towards higher 2θ angles, which is more emphasised in the mixture prepared with the trivalent *Ln* precursors (Figure 8a), as compared to the one of the precipitate prepared with UO_2^{2+}, Nd(III) and Ce(IV) (Figure 8b). This effect is also reflected in the intensities observed for the *Ln* phases, in the precipitate of the experiment with Ce(IV), where we can clearly distinguish between the three individual phases. For the $2UO_3 \cdot NH_3 \cdot 3H_2O$ and $NdCO_3OH$ (20.8 wt%) phases the reference pattern are clearly visible in the pattern of the precipitate and the CeO_2 phase (12.9 wt%) is reflected by the broadening around 28.6°, 33.1°, 47.5° and 56.3° 2θ. In contrast, the pattern of the precipitate prepared with Ce(III) does not allow to distinguish between the individual *Ln* phases, which indicates that a solid solution containing Nd and Ce might have formed. Due to the significantly lower intensity of the *Ln* phases a partial incorporation of the lanthanides into the ADU phase is expected.

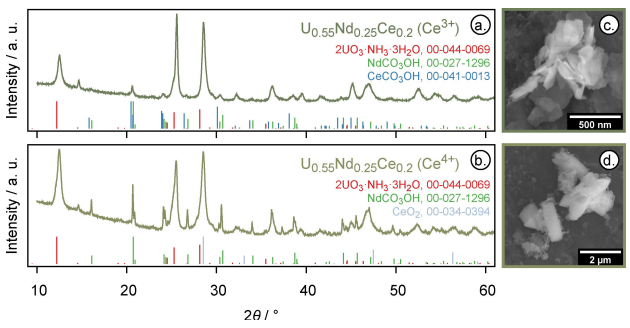

Figure 8. X-ray diffraction pattern and SEM micrographs obtained for the precipitates formed during the hydrolysis experiments for the ternary systems containing mixtures of UO_2^{2+}/Nd(III)/Ce(III) and UO_2^{2+}/Nd(III)/Ce(IV) with 55 mol%, 25 mol% and 20 mol% ($R=26$, 90 °C), as well as reference patterns originating from the PDF-2 database.[8,18–20]

2.2.2. SEM analyses

Representative SEM micrographs of the single component precipitates are presented as Figure 6g–l. Platelets differing in the geometrical shape were observed for all ADU phases of the single component precipitates. The experiment with $R=26$ at 100 °C led to almost squarish shaped grains with dimensions of about 4.5 µm×4.1 µm (Figure 6g), whereas the experimental conditions with $R=52$ at 90 °C resulted in a pronounced rectangular shape with a size of about 3.1 µm×1.4 µm (Figure 6h). The precipitate formed with $R=26$ at 90 °C showed hexagonal shaped platelets with about 790 nm in diameter and an edge length of about 440 nm on each side (Figure 6i). Grains with a typical orthorhombic shape were observed for the neodymium and cerium hydroxy carbonate precipitates formed from Nd(III) and Ce(III) ($R=26$, 90 °C). The length for the Ce(III) grains (Figure 6k) was up to about 2.5 µm, whereas the length of the Nd(III) grains (Figure 6j) were up to a factor of 100 smaller. For the Ce(IV) precipitate ($R=26$, 90 °C), randomly shaped agglomerates varying in size up to several µm were observed (Figure 6l), and the individual crystallites could not be distinguished.

Figure 7g–l shows the micrographs for the binary mixtures. For the mixtures of UO_2^{2+} and Nd(III) prepared with $R=52$, two different kind of grains could be identified (Figure 7g+h). This was much less pronounced for the precipitates formed with $R=26$, mainly randomly shaped platelets were observed (Figure 7i+j). Similar observations were made on the precipitates of the UO_2^{2+} and Ce(III) mixture (Figure 7k). Whereas the precipitate of the UO_2^{2+} and Ce(IV) mixture showed, randomly shaped agglomerates and a minor fraction of platelets.

The precipitate formed from UO_2^{2+}, Nd(III) and Ce(III) is presented in Figure 8c and consisted of randomly shaped platelets as well, no orthorhombic shaped grains were recognised during the analyses. Figure 8d shows the precipitate of

the UO_2^{2+}, Nd(III) and Ce(IV), in this case the presence of platelets and orthorhombic grains was observed.

3. Discussion

3.1. Uranyl/urea complexation

The UV/Vis results showed an absorption increase, paired with a shift of the uranyl absorption to a higher wavelength after urea addition (Figure 5a). This is in agreement with the visually observed colour intensification and indicates a complexation of the UO_2^{2+} ions and urea, which was reported by Collins et al.[22] in the context of IG and described in equation (2).

$$UO_2^{2+} + 2CO(NH_2)_2 \rightleftharpoons UO_2[CO(NH_2)_2]_2^{2+} \quad (2)$$

Collins et al.[22] reported about a stable complex at 0 °C, but a decomplexation occurred upon temperature increase. We did not observe a decomplexation in any of the samples taken at 90 °C after cooling to room temperature. However, our samples exhibit a large excess of urea (*R* of 26 or 52), shifting the equilibrium to the side of the complex. Moreover, we used significantly larger urea amounts as compared to IG processes, where *R* is generally between 0.8 and 2.2.[2]

3.2. Hydrolysis and single component precipitates

Theoretical hydrolysis pH values for the individual ions were calculated using *Chemical Equilibrium Diagrams* (Version 2020-Feb),[23] which is a derivative of *Spana* combined with a database formerly known as *Medusa/Hydra*.[24] The database contains logK values for room temperature. Consequently, the results are not directly applicable for the experimental conditions of this study, but allow to compare the observed trends. pH values of 3.48, 6.50 and 7.05 were calculated for $UO_3 \cdot 2H_2O_{(cr)}$, $Nd(OH)_{3\,(cr)}$ and $Ce(OH)_{3\,(cr)}$ formation from solutions containing 0.05 mol L^{-1} $UO_2(NO_3)_2$, $Nd(NO_3)_3$ and $Ce(NO_3)_3$, respectively. The database is incomplete for Ce(IV), but Marsac et al.[25] investigated its speciation in aqueous solution and demonstrated that the initially dominant $Ce^{4+}{}_{(aq)}$ species is converted with an increasing pH via $CeOH^{3+}$, $Ce(OH)_2^{2+}$ and $Ce(OH)_3^{+}$ into $Ce(OH)_{4\,(aq)}$. The latter starts to form at about pH 1.5 and at about pH 5 it is the only species present in aqueous solution.

3.2.1. Hydrolysis of uranyl ions

The ammonia consumption during precipitation results in a slower pH increase, as soon as all metal ions are precipitated the pH development is controlled by the decomposition of the remaining urea. The pH evolution implies for the hydrolysis experiments of uranyl an onset precipitation pH of about 4 for the three applied conditions (Figure 1), which is in agreement with the theoretical precipitation pH of 3.48. The precipitation was finished at a pH of about 5.3, confirmed by the absence of uranyl in the supernatant as the ICP-MS and UV/Vis results demonstrated (Figure 2). The reaction kinetics are controlled by the urea content and the temperature, with the latter having a larger influence. Compared to the hydrolysis carried out with $R = 26$ at 90 °C, the doubling in urea content caused the precipitation to be finished about twice as fast, while the temperature increase to 100 °C ($R = 26$) resulted in a precipitation in about a quarter of the time (Figure 1). Both parameters influenced also the stoichiometry and morphology of the ADU precipitate (Figure 6a–c). Cordfunke[26] performed detailed investigations on the ADU formation and identified four possible compounds, having the compositions and crystal system listed in Table 1.[18]

The lattice parameters of the monophasic $2UO_3 \cdot NH_3 \cdot 3H_2O$ (compound III, Table 1), formed at $R = 26$ at 90 °C ($a = b =$ 1.410(2) nm, $c = 1.451(2)$ nm), agree well to reference data of $a = b = 1.4087$ nm and $c = 1.4494$ nm[18] and the hexagonal shaped platelets observed by SEM (Figure 6i). For $R = 52$ (90 °C), a mixture of compound III and $3UO_3 \cdot NH_3 \cdot 5H_2O$ (compound II) was identified, whereas the hydrolysis at 100 °C ($R = 26$) resulted in a mixture of compound II and $UO_3 \cdot 2H_2O$ (compound I).

Cordfunke[26] demonstrated that $\frac{n(NH_3)}{n(UO_2^{2+})}$ in the solution defines the composition of the ADU precipitate. Compound I is formed up to a ratio of 0.011, when exceeding it, compound II starts to grow in. At a ratio of 0.333 only compound II is formed and at 0.382 (above pH 7) compound III is additionally generated, which is uniquely present beginning with a ratio of 0.730. Compound IV grows in if 0.829 is exceeded and occurs monophasic at a ratio of 33.25 and above. Manna et al.[27] confirmed the findings and observed for precipitates generated at pH 3.2 the presence of compound II, whereas precipitates formed at pH 3.5, 7.5 and 8.5 were multiphasic. They consisted of compounds II and III, having a larger fraction of III with increasing pH. In our work, $\frac{n(NH_3)}{n(UO_2^{2+})}$ changed as a function of time, since both, $n(UO_2^{2+})$ and $n(NH)$ decreased in the solution during precipitation,[23] whereas a constant amount of $n(NH_3)$ was continuously generated by the urea decomposition. All precipitates underwent a comparable pH evolution during the precipitation and the ICP-MS and UV/Vis results showed that the precipitation was completed at pH 5.3, consequently the formation of monophasic compound III precipitate is not explainable by the findings of Cordfunke.[26] The additional formation of compound I in the precipitate besides II, indicates that the reaction kinetics are controlling the precipitate composition, since it was the only difference between the uranyl experiments.

The morphology of ADU depends on many factors, such as the initial uranyl concentration and the temperature applied

Table 1. Solid NH_3–UO_3–H_2O phases[26] and their crystal systems.[18]

Compound	Composition	Crystal system
I	$UO_3 \cdot 2H_2O$	orthorhombic
II	$3UO_3 \cdot NH_3 \cdot 5H_2O$	orthorhombic
III	$2UO_3 \cdot NH_3 \cdot 3H_2O$	hexagonal
IV	$3UO_3 \cdot 2NH_3 \cdot 4H_2O$	orthorhombic

during its precipitation, but also the rotational speed and the shape of the impeller.[28] In terms of automation, a good powder flowability is desired and a large specific surface area increases the compressibility and sinterability, which is beneficial for converting the powder into pellets. Nkou Bouala et al.[11] used a hydrothermal method to precipitate uranium containing powders from uranyl nitrate by thermal decomposition of urea ($R=$ 83). They observed after 35 min and 45 min at 100 °C ADU nanospheres and after 55 min platelets. An increased temperature of 120 °C led to platelets already after 35 min. Their hexagonal platelets are similar in size to our hexagonal platelet precipitate (Figure 6i), since they did not identify the phases in their precipitates, no comparison to the formed compounds can be done.

None of the ADU precipitates from this work correspond to $3UO_3 \cdot 2NH_3 \cdot 4H_2O$ (compound IV), which was identified in ADU microspheres prepared by IG.[29] During the IG process, the precipitation occurs more rapidly and is accelerated by an additional thermal decomposition of hexamethylenetetramine (HMTA). Since four NH_4^+ ions are generated from one molecule of HMTA, a more significant pH increase is anticipated during the IG synthesis. Nevertheless, the absence of other ADU phases in the IG particles underline the assumption that the reaction kinetics impact the stoichiometry of the precipitated ADU composition.

3.2.2. Hydrolysis of Nd(III) and Ce(III)

The Nd(III) ions precipitated with absence of other metal ions between pH 5.9 and 6.3 (Figure 2a). For the binary mixtures of UO_2^{2+} and Nd(III) a larger precipitation pH range was determined. A urea content of $R=52$ led to Nd(III) precipitation between pH 4.9 and 6.8. For both Nd contents, 10 mol% and 25 mol% Nd, precipitation occurred after the precipitation of the uranyl ions. The reduction of urea ($R=26$) narrowed the Nd(III) precipitation region to a pH between 5.2 and 6.7, overlapping with the precipitation of UO_2^{2+} ions (Figure 3). For Ce(III) ions, an onset precipitation pH of 5.6 was observed, after 258 min no significant pH increase was determined (5.7), and about 60 % of the initially present Ce ions were precipitated (Figure 2a + b). The pH evolution implies a precipitation of the entire Ce(III) between 547 min and the final sample, at 547 min a pH of 6.3 was measured. In the binary mixture of UO_2^{2+} and Ce(III) also no endpoint for the Ce(III) precipitation was observed and about a quarter of the initial Ce was still present at pH 6.1. In the ternary experiments Nd(III) and Ce(III) behaved similarly, a decrease of both lanthanides in the solution was already observed at pH <5.9, but the major fraction precipitated above pH 5.9 until pH 6.7 was reached. For both trivalent lanthanides, a precipitation at lower pH values than the calculated theoretical values of 6.50 (Nd(III)) and 7.05 (Ce(III)) was observed.

Akinc and Sordelet[8] used a similar methodology with 0.025 mol L^{-1} metal cations, but varying urea contents. Experiments were performed with $Nd(NO_3)_{3\,(aq)}$ ($R\approx11$) and $Ce(NO_3)_{3\,(aq)}$ ($R\approx22$). They did not report a temperature, but stated that the solution was heated to mild boiling, implying that it was at a higher temperature than the 90 °C applied in our experiments with Nd(III) and Ce(III). Similar grain shapes were observed for the precipitates by SEM and orthorhombic $NdCO_3OH$ and $CeCO_3OH$ phases were identified for the precipitates. They determined for $NdCO_3OH$ lattice parameters of $a=0.4940$ nm, $b=0.8630$ nm, $c=0.7137$ nm, and for $CeCO_3OH$ $a=0.5018$ nm, $b=0.8566$ nm, $c=0.7384$ nm. Wang and Lu[10] performed hydrothermal hydrolysis experiments at 160 °C with $Ce(NO_3)_3$ and urea contents to R values of 1, 2, and 20. They noted that an increase in the urea led to larger particles. We determined lattice parameters of $a=0.503(4)$ nm, $b=0.849(8)$ nm, $c=0.733(6)$ nm for $NdCO_3OH$, and $a=0.500(2)$ nm, $b=0.856(4)$ nm, $c=0.731(2)$ nm for $CeCO_3OH$. The lattice parameters for $CeCO_3OH$ match well to those determined by Akinc and Sordelet,[8] whereas the differences for the $NdCO_3OH$ phase is larger, which might be due to different crystallite sizes as result of the lower urea content, as implied by the findings of Wang and Lu.[10]

For trivalent Am and Pu a similar precipitation behaviour compared to Nd and Ce is anticipated. Slightly lower theoretical hydrolysis pH values of 6.23 were calculated for both actinides using the mentioned software package and molar metal concentrations of 0.05 mol L^{-1}.[23]

3.2.3. Hydrolysis of Ce(IV)

The precipitation of Ce(IV) occurred between pH 1.3 and 2.9 (Figure 2a), which agrees to the calculations made by Marsac et al.[25] In the binary system (20 mol% Ce), a slightly increased onset precipitation pH of 2.0 was observed, which further increased for the ternary system, where the Ce(IV) precipitation was observed between pH 2.2 and 4.3. This is most likely caused by the other components, having a higher initial pH.

The precipitation behaviour anticipated for Pu(IV) is comparable to Ce(IV), but shifted towards higher pH. The formation of $Pu(OH)_{4\,(aq)}$ was determined for a pH above $\approx$4.5 by Marsac et al.[25]

3.3. Precipitates of the binary and ternary systems

In the binary UO_2^{2+}/Nd(III) system, the large urea excess of $R=$ 52 is less favourable for a co-precipitation, which was partially observed for $R=26$ (Figure 3). Individual $NdCO_3OH$ phases were less pronounced in the precipitate formed with $R=26$ (Figure 7a–d). Those results imply that the urea content has an impact in the product homogeneity. The usage of Ce(III) in the binary UO_2^{2+}/Ce(III) system ($R=26$) led to a comparable precipitate as observed for Nd(III) (Figure 7d + e). In the case of doped ADU gels, prepared by IG, no individual *Ln* phases were determined by XRD for dopant contents up to 30 mol% prepared with Nd(III) or Ce(III) precursors.[6,30] The negative influence of Ce(IV) on the crystallinity of the ADU precipitate (Figure 7f) was observed for a tetravalent Ce precursor during the preparation of Ce-doped ADU gels by IG as well.[6,30]

In the ternary system, a simultaneous precipitation of Nd(III) and Ce(III) was observed (Figure 4a + b). A large fraction of the resulting *Ln* phase was incorporated in the ADU phase (Figure 8a), while for the ternary system with Ce(IV), three individual phases were formed during the precipitation (Figure 4c + d), which were also identified in the product (Figure 8b). Consequently, Ce(III) is better suitable for the production of Ce-doped ADU than Ce(IV), a lower pH difference has to be overcome to complete the precipitation, resulting in a smaller *R*. In addition, a better homogeneity of the formed product is anticipated, which might further enhance due to the smaller *R*.

A hydrothermal approach should be studied for the production of MA containing transmutation fuel pellets. Well-chosen urea contents, reaction times and temperatures might lead to nanospheres instead of platelets,[11] which should be due to a larger reactive area beneficial in terms of compressibility and sinterability to obtain homogeneous fuel pellets.

4. Conclusion

Within this study, a complexation between UO_2^{2+} and urea was proven by UV/Vis, which did not occur for Nd(III) and urea. The hydrolysis of UO_2^{2+} at 90 °C and 100 °C occurred between pH 4.5 and 5.3 and the urea content, as well as the temperature control the reaction kinetics, which influenced the product composition. ADU precipitates of different stoichiometry formed and multiphasic products but also a monophasic product were determined, dependent on the different experimental parameters. A similar pH evolution was observed for Nd(III) and Ce(III) with a precipitate forming between pH 5.2 and 6.7. The precipitates were identified as $NdCO_3OH$ and $CeCO_3OH$, respectively. For Ce(IV), the hydrolysis took place between pH 1.3 and 2.9 and a nanocrystalline CeO_2 phase formed. In mixtures of uranyl and the lanthanide ions, the general precipitation regions were confirmed. Slight shifts to higher hydrolysis pH values were observed for ions in mixtures with the presence of ions with higher initial pH values. For binary mixtures of UO_2^{2+} and Nd(III) a co-precipitation was partially observed for $R = 26$, which did not occur for a higher urea content of $R = 52$, revealing an influence of the urea content on the homogeneity of the precipitate, which might be caused by a more stable uranyl/urea complex due to the larger urea content. The different phases identified for Ce(III) and Ce(IV) were also determined in the precipitates of binary uranyl and cerium mixtures. Moreover, the crystallinity of the ADU phase was negatively impacted in the precipitate formed in presence of Ce(IV)/CeO_2. A simultaneous precipitation of Nd(III) and Ce(III) was observed for the ternary compositions and a certain fraction of the *Ln* phase was probably also incorporated in the ADU phase, while the precipitation with presence of Ce(IV)/CeO_2 led to three individual phases. The results explain the differences observed during the fabrication, but also the thermal treatment of Ce-doped particles prepared by IG with trivalent and tetravalent dopant precursors. We demonstrated a suitability of the method to prepare precursors for the production of MA containing transmutation fuel, but the thermal decomposition of the precipitates should be further studied. Moreover, a hydrothermal approach for the fabrication of doped ADU might be promising, since a powder morphology better suitable with respect to sinterability and pelletisation is anticipated.

Experimental

Chemicals

Uranyl nitrate was prepared from $UO_{2.06(1)}$ depleted in U-235 (0.3 g/100 g U, provided by AREVA). Impurities were analysed and found to be < 0.01 wt%. The trivalent lanthanide nitrates, $Nd(NO_3)_3 \cdot 6H_2O$ and $Ce(NO_3)_3 \cdot 6H_2O$, were ordered from Strem Chemicals Inc. (≥ 99.9 wt%). Diammonium cerium(IV) nitrate ($(NH_4)_2[Ce(NO_3)_6]$, for analysis, 99.5 wt%), originated from Acros Organics and nitric acid ($w(HNO_3) =$ 70 wt%; ≥ 99.999 wt%; trace metals basis) was purchased from Aldrich. Ammonia solution ($w(NH_3) = 28$ wt% to 30 wt%; ACS reagent®) and urea (pellets; ≥ 99.5 wt%; ReagentPlus®) were ordered from Sigma-Aldrich.

Precipitation of powders

Preparation of uranyl nitrate

UO_{2+x} was dissolved in stoichiometric amounts of HNO_3 to form a uranyl nitrate solution (UNS). The solution was evaporated on a heating plate while stirring with a glass rod. The obtained crystals were dried for 24 h at a pressure of 50 mbar (25 °C), about 40 g uranyl nitrate ($UO_2(NO_3)_2 \cdot xH_2O$) was prepared.

Preparation of metal precursor solutions

UNS was prepared by dissolving $UO_2(NO_3)_2 \cdot xH_2O$ in ultrapure water. A volume of 25 mL UNS was generated and based on the mass of uranyl nitrate, a molar uranium concentration of 1.4(1) mol L^{-1} was assumed. Lanthanide precursor solutions were prepared by dissolving the corresponding salt ($Nd(NO_3)_3 \cdot 6H_2O$, $Ce(NO_3)_3 \cdot 6H_2O$ and $(NH_4)_2[Ce(NO_3)_6]$) in ultrapure water. Volumes of 10 mL were produced for each precursor and molar concentrations of 0.55(5) mol L^{-1}, 0.11(1) mol L^{-1} and 0.11(1) mol L^{-1} were assumed for the metals, respectively.

Hydrolysis experiments

The hydrolysis experiments were carried out in a 100 mL three neck round bottom flask, equipped with a cooler in the middle and a thermocouple (−200 °C to 1370 °C) on one side. The third neck was closed with a plug, which was removed for sampling during the experiments. The cooler was connected to a chiller (Buchi, F-105), set to 9 °C, and the thermocouple to a thermometer (Ludwig Schneider Digital-Measuring Instrument 65625). The flask was placed in an oil bath with a magnetic stir bar. It was temperature controlled by a heating and stirring plate equipped with a thermocouple (VWR adv. VMS-C7). A photograph of the set-up is included in the dataset of this study (Figure 2 within Ref. 13).[13] Each hydrolysis experiment was carried out using 50 mL solution aiming at a total metal concentration of 0.05 mol L^{-1}. The solution was prepared by mixing appropriate volumes of the precursor solutions and diluting the blend with ultrapure water, except for the experiments conducted with lanthanides only. For the latter it was prepared by weighing the desired mass of the corresponding compound into a 50.00(4) mL volumetric flask and dissolving it in ultrapure water. After addition to the flask, the solution was gently stirred using a magnetic stir bar and the oil bath was heated to the

desired temperature. The experiments were carried out at 90 °C and one additional experiment containing only uranyl nitrate was done at 100 °C. Upon reaching the desired temperature, an initial sample of 2 mL was taken and solid urea was added to the flask after sampling, which dissolved rapidly (< 1 min). We express the amount of urea as R, corresponding to the $\frac{n(\text{urea})}{n(M^{n+})}$ ratio. Since we aimed for molar metal concentrations of 0.05 mol L^{-1} in all experiments, constant masses of urea were required for each of the ratios. We performed experiments with $R = 26$ (m(urea) = 3.754 g) and the urea was weighed using a Mettler-Toledo AG204 balance. To investigate the influence of the urea concentration, some experiments were additionally done with $R = 52$ (m(urea) = 7.508 g). The time of urea addition was used as reference time for further evaluation of the experiment ($t = 0$). Within the course of about 10 h, 2 mL samples were taken every 25 min to 50 min. Afterwards, the experiment was kept stirring at the desired temperature for about 25 h in total (1500(60) min), then a final sample was taken.

Additionally, one experiment was performed without metal ions, using only urea dissolved in ultrapure water to monitor the changes in pH during its decomposition. This experiment was performed with a mass of urea equal to the amount used in the $R = 26$ experiments.

All data collected during the preparation and sampling for each of the experiments, like the precursor solution volumes, the urea masses, and the addition times, as well as the sampling times are included in the dataset of this study.[13]

Post treatment

The formed precipitate and the remaining supernatant were centrifuged for 15 min at 6500 rpm. Then, the supernatant was removed from the centrifuge vials. In order to remove water-soluble by-products (e.g. NH_4NO_3), the precipitate was washed with ultrapure water. The resulting suspension was centrifuged for another 15 min at 6500 rpm. This procedure was repeated three times. After the last washing step, the water was removed and the precipitate was dried at 40 °C and 250 mbar for multiple days until a stable mass was observed.

Characterisation

pH measurements

The pH of the samples taken during the hydrolysis experiments was measured using a precision pH meter (WTW, pH 3110), utilising a SenTix® 41 probe. Calibrations were carried out on daily basis with pH 4.01 and pH 7.00 technical buffer solutions (WTW, TEP 4 and TEP 7). The measurements were performed after the samples cooled to temperatures between 25 °C and 29 °C.

Inductive coupled plasma mass spectrometry

Metal concentrations in the hydrolysis samples were determined by ICP-MS. An ELEMENT 2 system (Thermo Scientific) was calibrated with 1 ppb, 2 ppb, 5 ppb, 10 ppb and 20 ppb standard solutions, prepared from a 1000 ppm single element standard (SPEX, CertiPrep) diluted with a matrix consisting of ultrapure water and HNO_3 (2% V/V). Dilution factors between $1:10^3$ and $1:10^6$ were applied to the sample solutions. The directly measured mass concentrations have a relative uncertainty of 10% (2σ) and were converted into the molar concentrations.

Ultraviolet-visible spectroscopy

To evaluate the metal concentration in the hydrolysis samples, UV/Vis measurements were performed, using a Shimadzu UV-2600 spectrophotometer. The samples were transferred into 700 µL quartz glass cuvettes (Hellma, 104-002-10-40) and a wavelength range from 185 nm to 900 nm was measured with a step size of 1 nm. Data acquisition was performed with the software package *UVProbe* by Shimadzu (Version 2.62).

X-ray powder diffraction

XRD analyses were carried out using a PANalytical X'Pert Pro diffractometer. The device utilises a Bragg-Brentano parafocusing geometry in a θ-θ configuration. A sintered, high purity Si disc was used for zero point calibration. Weekly validations were performed on a sintered Al_2O_3 disc (NIST Standard Reference Material 1976b). Lattice parameter refinement of Si was done to assess the instrument bias, which was found to be smaller than 10^{-5} relative (1σ). A copper LFF X-ray tube ($K\alpha_1 = 1.5405929$ Å)[31] was used as radiation source. The measurement of high-quality diffractograms with low axial divergence was ensured by a combination of a fixed divergence slit, 0.02 rad soller slits and a copper beam mask. The diffracted beam path was foreseen with a Ni filter and detection was done with a position-sensitive detector (PANalytical X'Celerator).

Sample material was placed on a specimen holder using the back loading preparation technique. For experiments where an insufficient amount of precipitate was formed, a suspension of sample material in ethanol was dropped onto a zero background silicon single crystal holder. All diffractograms were recorded from 10° to 80° 2θ with a step size of 0.017°. Lattice parameter determination was performed with the unit cell refinement option of *HighScore Plus* (PANalaytical, Version 4.8), which applies the method described by Nelson and Riley.[32]

Scanning electron microscopy

SEM analyses were done using a Jeol JSM 7100FA field-emission microscope, equipped with a secondary and backscattered electron detector. The working distance ranged from 7 mm to 10 mm and an accelerating voltage of 15 kV was employed. A suspension of the sample material in ethanol was drop-wise given to an aluminium specimen holder and the sample holder was loaded into the device after evaporation.

Acknowledgements

Financial support for this research was provided by the European Commission (project: GENIORS-GEN IV Integrated Oxide fuels Recycling Strategies (grant number 755171)) and by the Belgian FPS Economy (project: ASOF – Advanced Separation for Optimal management of spent Fuel). The authors thank K. Vanaken and P. Dries for laboratory assistance, C. Odeurs for support with UV/Vis measurements and P. Verheyen for ICP-MS analyses. Special thanks to Dr. S. Finkeldei for reviewing this manuscript. Open Access funding enabled and organized by Projekt DEAL.

Data Availability Statement

The data required to reproduce the findings of this study can be downloaded from the Zenodo repository (https://doi.org/10.5281/zenodo.3841374, license: CC BY-NC).[13]

Conflict of Interest

The authors declare no conflict of interest.

Keywords: Ammonium diuranate · Cerium · Co-conversion · Neodymium · Uranium

[1] M. Salvatores, G. Palmiotti, *Prog. Part. Nucl. Phys.* **2011**, *66*, 144–166.
[2] V. N. Vaidya, *J. Sol-Gel Sci. Technol.* **2008**, *46*, 369–381.
[3] M. A. Pouchon, G. Ledergerber, F. Ingold, K. Bakker in *Comprehensive Nuclear Materials*, R. J. Konings (Ed.), Elsevier BV, Oxford, **2012**, chapter 3.11, pp. 275–312.
[4] S. Suryanarayana, N. Kumar, Y. R. Bamankar, V. N. Vaidya, D. D. Sood, *J. Nucl. Mater.* **1996**, *230*, 140–147.
[5] C. Schreinemachers, A. A. Bukaemskiy, M. Klinkenberg, S. Neumeier, G. Modolo, D. Bosbach, *Prog. Nucl. Energy* **2014**, *72*, 17–21.
[6] C. Schreinemachers, G. Leinders, G. Modolo, M. Verwerft, K. Binnemans, T. Cardinaels, *J. Nucl. Mater.* **2020**, *535*, 152128.
[7] C. Schreinemachers, G. Leinders, R. Podor, J. Lautru, N. Clavier, G. Modolo, M. Verwerft, K. Binnemans, T. Cardinaels, *J. Nucl. Mater.* **2020**, *542*, 152454.
[8] M. Akinc, D. Sordelet, *Adv. Ceram. Mater.* **1987**, *2*, 232–238.
[9] G. J. d. A. A. Soler-Illia, M. Jobbágy, A. E. Regazzoni, M. A. Blesa, *Chem. Mater.* **1999**, *11*, 3140–3146.
[10] H.-C. Wang, C.-H. Lu, *Mater. Res. Bull.* **2002**, *37*, 783–792.
[11] G. I. Nkou Bouala, N. Clavier, R. Podor, J. Cambedouzou, A. Mesbah, H. P. Brau, J. Lechelle, N. Dacheux, *CrystEngComm* **2014**, *16*, 6944–6954.
[12] T. Wangle, V. Tyrpekl, T. Delloye, O. Larcher, J. Pakarinen, T. Cardinaels, J. Vleugels, M. Verwerft, *Radiochim. Acta* **2018**, *106*, 645–653.
[13] C. Schreinemachers, O. Bollen, G. Leinders, *Data of uranyl-, Nd-, Ce-hydrolysis and their mixtures induced by thermal decomposition of urea*, **2021**, (Version 1.0.0) [Data set], License: CC BY-NC, https://doi.org/10.5281/zenodo.3841374.
[14] C. Veranitisagul, A. Kaewvilai, S. Sangngern, W. Wattanathana, S. Suramitr, N. Koonsaeng, A. Laobuthee, *Int. J. Mol. Sci.* **2011**, *12*, 4365–4377.
[15] M. Bravo, A. C. Olwiert, B. Oelckers, *J. Chil. Chem. Soc.* **2009**, 54.
[16] D. Hong, M. Murakami, Y. Yamada, S. Fukuzumi, *Energy Environ. Sci.* **2012**, *5*, 5708–5716.
[17] V. Shah, S. Shah, H. Shah, F. J. Rispoli, K. T. McDonnell, S. Workeneh, A. Karakoti, A. Kumar, S. Seal, *PLoS One* **2012**, *7*, e47827.
[18] P. C. Debets, B. O. Loopstra, *J. Inorg. Nucl. Chem.* **1963**, *25*, 945–953.
[19] H. Dexpert, P. Caro, *Mater. Res. Bull.* **1974**, *9*, 1577–1585.
[20] M. C. Morris, H. F. McMurdie, E. H. Evans, B. Paretzkin, H. S. Parker, N. P. Pyrros, C. R. Hubbard, in *National Bureau of Standards*, Vol. 25, National Bureau of Standards, **1984**.
[21] G. K. Williamson, W. H. Hall, *Acta Metall.* **1953**, *1*, 22–31.
[22] J. L. Collins, M. F. Lloyd, R. L. Fellows, *Radiochim. Acta* **1987**, *42*, 121–134.
[23] I. Puigdomènech, *Chemical Equilibrium Diagrams for aqueous systems*, Github, **2020**, https://github.com/ignasi-p/eq-diagr.
[24] I. Puigdomènech, E. Colàs, M. Grivé, I. Campos, D. García in *MRS Proceedings*, Cambridge University Press (CUP), **2014**, pp. 111–116.
[25] R. Marsac, F. Réal, N. L. Banik, M. Pédrot, O. Pourret, V. Vallet, *Dalton Trans.* **2017**, *46*, 13553–13561.
[26] E. H. P. Cordfunke, *J. Inorg. Nucl. Chem.* **1962**, *24*, 303–307.
[27] S. Manna, R. Kumar, S. K. Satpati, S. B. Roy, J. B. Joshi, *Nucl. Eng. Technol.* **2017**, *49*, 541–548.
[28] S. Manna, C. Basak, U. R. Thakkar, S. Thakur, S. B. Roy, J. B. Joshi, *J. Radioanal. Nucl. Chem.* **2016**, *310*, 287–299.
[29] C. Schreinemachers, G. Leinders, G. Modolo, M. Verwerft, K. Binnemans, T. Cardinaels, *Nucl. Eng. Technol.* **2020**, *52*, 1013–1021.
[30] C. Schreinemachers, G. Leinders, *Characterisation data of Nd- and Ce-doped uranium dioxide microspheres prepared via internal gelation*, **2020**, (Version 1.0.0) [Data set], License: CC BY-NC, https://doi.org/10.5281/zenodo.3560620.
[31] J. Härtwig, G. Hölzer, E. Förster, K. Goetz, K. Wokulska, J. Wolf, *Phys. Status Solidi A* **1994**, *143*, 23–34.
[32] J. B. Nelson, D. P. Riley, *Proc. Phys. Soc.* **1945**, *57*, 160–177.

Manuscript received: May 23, 2021
Revised manuscript received: June 29, 2021
Accepted manuscript online: July 22, 2021